

SANDIA REPORT

SAND2000-2882

Unlimited Release

Printed November 2000

Optical Interconnections to Focal Plane Arrays

Jeffrey L. Rienstra and Michael K. Hinckley

Prepared by
Sandia National Laboratories
Albuquerque, New Mexico 87185 and Livermore, California 94550

Sandia is a multiprogram laboratory operated by Sandia Corporation,
a Lockheed Martin Company, for the United States Department of
Energy under Contract DE-AC04-94AL85000.

Approved for public release; further dissemination unlimited.



Issued by Sandia National Laboratories, operated for the United States Department of Energy by Sandia Corporation.

NOTICE: This report was prepared as an account of work sponsored by an agency of the United States Government. Neither the United States Government, nor any agency thereof, nor any of their employees, nor any of their contractors, subcontractors, or their employees, make any warranty, express or implied, or assume any legal liability or responsibility for the accuracy, completeness, or usefulness of any information, apparatus, product, or process disclosed, or represent that its use would not infringe privately owned rights. Reference herein to any specific commercial product, process, or service by trade name, trademark, manufacturer, or otherwise, does not necessarily constitute or imply its endorsement, recommendation, or favoring by the United States Government, any agency thereof, or any of their contractors or subcontractors. The views and opinions expressed herein do not necessarily state or reflect those of the United States Government, any agency thereof, or any of their contractors.

Printed in the United States of America. This report has been reproduced directly from the best available copy.

Available to DOE and DOE contractors from
U.S. Department of Energy
Office of Scientific and Technical Information
P.O. Box 62
Oak Ridge, TN 37831

Telephone: (865)576-8401
Facsimile: (865)576-5728
E-Mail: reports@adonis.osti.gov
Online ordering: <http://www.doe.gov/bridge>

Available to the public from
U.S. Department of Commerce
National Technical Information Service
5285 Port Royal Rd
Springfield, VA 22161

Telephone: (800)553-6847
Facsimile: (703)605-6900
E-Mail: orders@ntis.fedworld.gov
Online order: <http://www.ntis.gov/ordering.htm>



SAND2000-2882
Unlimited Release
Printed November 2000

Optical Interconnections to Focal Plane Arrays

Jeffrey L. Rienstra and Michael K. Hinckley
Space Sensor Engineering Department
Sandia National Laboratories
P.O. Box 5800
Albuquerque, New Mexico 87185-0972

Abstract

We have successfully demonstrated an optical data interconnection from the output of a focal plane array to the downstream data acquisition electronics. The demonstrated approach included a continuous wave laser beam directed at a multiple quantum well reflectance modulator connected to the focal plane array analog output. The output waveform from the optical interconnect was observed on an oscilloscope to be a replica of the input signal. We fed the output of the optical data link to the same data acquisition system used to characterize focal plane array performance. Measurements of the signal to noise ratio at the input and output of the optical interconnection showed that the signal to noise ratio was reduced by a factor of 10 or more. Analysis of the noise and link gain showed that the primary contributors to the additional noise were laser intensity noise and photodetector receiver noise. Subsequent efforts should be able to reduce these noise sources considerably and should result in substantially improved signal to noise performance. We also observed significant photocurrent generation in the reflectance modulator that imposes a current load on the focal plane array output amplifier. This current loading is an issue with the demonstrated approach because it tends to negate the power saving feature of the reflectance modulator interconnection concept.

Acknowledgments

The authors thank Marcelino Arnedariz and Gary Schuster of RF and Opto Microsystems Department for use of their laboratory and assistance with the preliminary concept demonstration using the modulator/retroreflector.

We thank Colin Smithpeter of Advanced Military Systems Department for use of the reflectance modulator used in our breadboard optical interconnect system.

We also thank Rex Kay of Space Sensor Engineering Department for many useful comments during the preparation of this report.

Contents

Introduction.....	7
Optical Interconnect Concept.....	7
Motivation for optical interconnect.....	7
Candidate concepts	8
Selected optical interconnect concept.....	9
Preliminary Concept Demonstration.....	11
Retroreflector modulator.....	11
Results of preliminary demonstration.....	12
Optical Interconnect Breadboard	14
Breadboard description.....	14
Reflectance modulator	16
Laser diode source	20
Fiber optics.....	22
Photodetector	22
Measured Breadboard Performance.....	23
Analysis of Measurements.....	26
Calculated signal swing.....	26
Calculated noise	27
Potential performance improvement	30
Suggestions for Further Work.....	31
Improved source.....	31
Improved modulator.....	31
Lower noise detector.....	32
Design tradeoffs	32
Summary and Conclusions.....	32

Figures

Figure 1. Optical interconnection concept	10
Figure 2. Modulator/retroreflector concept diagram.....	12
Figure 3. Preliminary concept demonstration.....	12
Figure 4. Modulator/retroreflector transfer function.....	14
Figure 5. Optical interconnect breadboard concept.....	15
Figure 6. Optical interconnect breadboard setup	16
Figure 7. Close-up of reflectance modulator.....	16
Figure 8. Modulator reflectance versus wavelength.....	17
Figure 9. Modulation factor versus wavelength.....	18
Figure 10. Modulator reflectance versus voltage at 849 nm.....	19
Figure 11. Reflectance modulator capacitance versus wavelength.....	19
Figure 12. Modulator spectral quantum efficiency at 2 volts reverse bias	20
Figure 13. Laser diode output wavelength versus temperature.....	21
Figure 14. Optical interconnect output and DART focal plane output	23
Figure 15. Output traces at 1 megapixel/second	24
Figure 16. Expanded 1 megapixel/second output trace.....	25
Figure 17. Noise squared versus signal swing squared.....	28
Figure 18. Components of squared noise.....	29
Figure 19. Component SNR versus output signal swing.....	31

Tables

Table 1. Optical Power Measurements	13
Table 2. Laser Noise Measurements.....	22
Table 3. DART FPA Signal and Noise Levels.....	26
Table 4. Optical Interconnect Signal and Noise Levels.....	26

Introduction

As focal plane arrays for satellite sensor systems become larger and faster, the power required for output signal drivers becomes a limiting factor. When large format, fast framing arrays must be cooled to cryogenic temperature, the power required to drive multiple output signals across low thermal conductance cryogenic cables becomes a significant fraction of the total cooling load. While advances in microelectronics technology promise further reductions in device size and electrical power dissipation, the power required to drive off-chip capacitive loads will remain nearly constant. In next generation sensor system concepts, nearly one third of the electrical power dissipation of the focal plane array is consumed in output signal drivers. This fraction will most likely continue to increase with larger and faster focal plane arrays. By using optical interconnections for the signal outputs, the active power dissipation of the focal plane array can be reduced.

The objective of this project was to identify and refine candidate optical interconnection concepts and to demonstrate the selected concept. Several approaches for an optical data link are possible. An optical source can be located on the cold focal plane and directly modulated with the output signal voltage. Another choice involves the use of optical fibers or free space transmission across the warm-cold interface. The approach selected for this effort uses an optical source and receiver on the warm side of the interface, where power dissipation is not as critical as on the cryogenic side. A very low power optical modulation device on the cold side of the interface impresses the focal plane output signal on a free space optical beam. Demonstration of this concept was dependent upon the availability of the necessary components, and the optical modulator was the critical component for this approach. Fortunately, we were able to obtain a Fabry-Perot reflectance modulator fabricated here at Sandia. Other components for this concept are commercially available

Optical Interconnect Concept

Motivation for optical interconnect

There are a number of potential advantages for the use of optical data links to focal plane arrays. As demonstrated with optical communications systems, very high data rates are possible with direct modulation of semiconductor laser sources or with the use of high speed external modulators. Total data throughput can be multiplied with the use of wavelength division multiplexing. There is great potential to leverage technology developed for the optical communications industry. As focal plane arrays become larger and denser in pixels and the frame rates continue to increase, the tremendous data rates required could very well favor optical data interconnections.

Another possible advantage of optical interconnections to focal plane arrays is the promise of reduced power consumption. This consideration is most applicable for high performance infrared focal plane arrays operating at cryogenic temperature. A large format, fast framing focal plane array typically has multiple analog output channels to keep the output pixel rate per channel at a reasonable level. Current technology typically limits the output pixel rate per channel to 5 to 10 million pixels per second. These output signal channels are usually digitized to 12 bits.

Focal plane arrays contemplated for next generation space systems will have several million pixels with frame rates in the neighborhood of 100 frames per second. For example, a 3 million pixel array operating at 100 frames per second would require 30 output channels, each running at 10 megapixels per second. The power required to drive so many output channels becomes a significant portion of the total electrical power dissipation. Output amplifiers consume anywhere from a few milliwatts up to 10 milliwatts, depending on the amplifier design, output pixel rate, and load impedance. The 150 mW of power generated by 30 outputs at 5 mW each is a significant fraction of the total active power dissipation of the focal plane array which must be handled by the cryocooling system.

For a cryogenically cooled focal plane, conventional electrical interconnections present a substantial capacitive load to the output driver amplifiers. Special cables are used for these electrical interconnections that balance the need for low thermal conductance with adequate electrical conductance. Unfortunately, such cryocables typically have higher capacitance per unit length than conventional electrical cables, and usually a longer length than required by interconnect distance is used. Despite continuing advances in microelectronics technology and power reductions due to smaller device geometries and lower supply voltages, the power demanded to drive cryogenic electrical cables will remain nearly constant.

The total payload power available must also be considered in sensor system design. Cooling power available to a cryogenic temperature focal plane array for a satellite sensor system is often severely limited. Although long-life, space-qualified cryocooler technology is advancing steadily, there is a limit to the total cooling power available at a given operating temperature. For current cryocooler technology using typical infrared focal plane operating temperatures and cooling loads, the ratio of cryocooler input power to focal plane cooling load is in the range of 10 to 40.

There is, therefore, strong incentive to reduce the cooling load presented by the focal plane array and to move as much electrical power dissipation as possible off the cold focal plane. The principal motivation for this project was to investigate a concept for decreasing the power required to couple the focal plane output signal to the downstream signal processing electronics.

Candidate concepts

There are a number of possible approaches for optical interconnection of focal plane output signals to other electronics. The most straightforward approach is to place an optical source, such as a light emitting diode or laser diode, on the focal plane for each output channel and drive it directly with its respective signal. The intensity modulated optical signal is picked up on the warm side of the interface and converted back to voltage.

Another approach is to locate the optical source off the focal plane on the warm side of the interface. A continuous wave (CW) laser source is directed at the focal plane and some sort of optical modulator is used to encode the focal plane output signal onto the optical beam. Either a transmission type or reflection type modulator could be used.

A third option for the optical interconnection approach involves the type of optical beam transmission to use, either free space or optical fiber. Both approaches have advantages and disadvantages to be evaluated. Considerations include ease of alignment, susceptibility to vibration, stray light rejection, and coupling efficiency.

A fundamental choice regarding an optical data link is whether to use digital or analog signal transmission. Most optical data communication applications use digital encoding. While analog-to-digital (A-to-D) conversion on the focal plane offers some advantages in the areas of noise reduction and immunity to interference, cryogenic focal plane outputs are usually implemented in the analog domain. The power required to operate A-to-D converters on a cryogenic focal plane is prohibitive for most applications, especially for large format, fast framing detector arrays. Analog optical transmission presents its own set of challenges, including stringent linearity and noise requirements.

Selection of the optimum approach for any given focal plane application would involve a number of factors and detailed analysis. For this breadboard demonstration, we chose to use an off focal plane optical source and a reflectance modulator. We believed that a modulator, rather than a directly driven optical source on the focal plane, promised the lowest power operation. Optical transmission for the breadboard demonstration combined fiber optic and free space portions, with the assumption that the warm-cold interface would be spanned with a free space beam. Finally, we chose analog signal transmission because it appears to be the more power efficient approach.

Selected optical interconnect concept

A simple diagram of how an optical interconnection concept might work in a system is shown in Figure 1. The diagram shows a cryogenically cooled focal plane array with each output channel connected to a reflectance modulator. The reflectance of each modulator is a function of the signal voltage. On the warm side of the interface are laser diode optical sources and photoreceivers corresponding to each of the reflectance modulators. Since the optical sources are on the warm side, the power required to operate them is not of critical importance. It is assumed that the power required to drive the reflectance modulators is very small, on the order of microwatts. If the reflectance modulators are made small, their capacitive load presented to the focal plane output amplifiers should be very small.

The critical component for this optical data link concept is the reflectance modulator. These devices are under study by Sandia National Laboratories for a number of applications, and Sandia is able to fabricate them in its Compound Semiconductor Research Laboratory. The devices utilize multiple quantum well (MQW) diode structures with device parameters tailored to provide response over a narrow wavelength range, typically a few nanometers. A Fabry-Perot cavity is formed in the intrinsic layer of the PIN diode between two reflector stacks. The reflectance of the device can be varied in this narrow wavelength range by applying different levels of reverse bias to the diode. The reflectance of the device at the operating wavelength can be changed substantially, 50 % or so, with only a few volts of applied bias. With a depth of optical modulation in this range, the DC pedestal on which the modulated signal rests remains manageable. The speed of operation of these reflectance modulators depends on device capacitance and can be as high as 50 MHz for devices 500 micrometers in diameter.

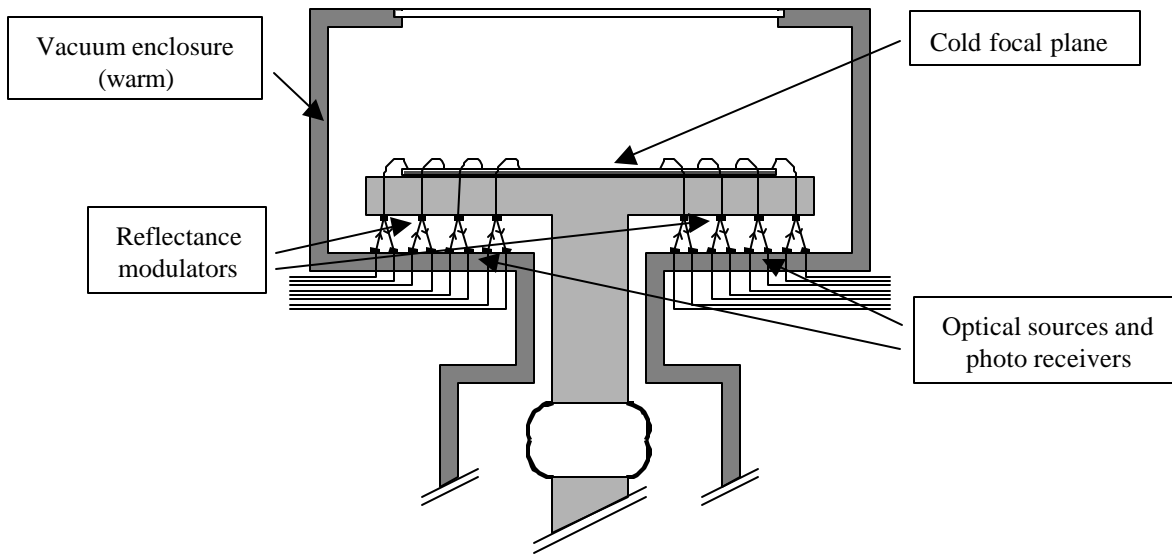


Figure 1. Optical interconnection concept

Since the operating wavelength range of MQW reflectance modulators is a few nanometers, a laser optical source is required with relatively tight wavelength control. For greatest efficiency and compact design, semiconductor diode laser sources are preferred. Because the output wavelength of laser diodes is a function of temperature, active temperature control using a thermoelectric cooler with temperature sensor feedback is most likely necessary. In addition, the temporal stability of the laser intensity must be very good. Semiconductor diode lasers are very sensitive to feedback instability and mode hopping, and this fact was observed in our investigation.

The voltage input requirements for the reflectance modulator match well with the signal output voltage of focal plane arrays. Many modern focal plane arrays operate from 5 volt power supplies and have an output signal ranging anywhere between 1 and 4 volts. For a given detector array the signal swing between the dark level and the saturation level is in the neighborhood of 2 volts. Very little gain or offset adjustment is required to interface a focal plane output to the input of a reflectance modulator.

The photodetector is also a key component and must be designed to minimize its addition to the total noise of the optical interconnection. A common photodetector design uses a semiconductor photodiode coupled with a transimpedance amplifier to produce a voltage proportional to the optical power incident on the detector. The responsivity (amps/watt) of the photodiode depends on its quantum efficiency and the wavelength of the optical signal. The value of the feedback resistor of the transimpedance amplifier sets the transimpedance gain (volts/amp) and is selected to match the desired output voltage with the expected photocurrent. There is a tradeoff between maximum transimpedance gain and speed of response, so the input optical power must be large enough to produce the desired output voltage at the required speed.

For an actual focal plane optical interconnection application all these component requirements need to be considered for an optimum design. To make the optical link more compact, the laser diode sources and photodiode receivers could be built on the same substrate. The operating wavelength of the reflectance modulator could be selected to be below the spectral range of the focal plane array. Allowance would need to be made for the shift in operating wavelength as the modulator is cooled to cryogenic temperature. The mechanical structure for the optical components would be designed to maintain accurate alignment and to minimize the effects of vibration. For the optical interconnection demonstration under this project, many of these detailed design considerations were deferred because they were not essential to establishing the feasibility of the approach.

Preliminary Concept Demonstration

Retroreflector modulator

As work began on this project we became aware of a related Sandia project to demonstrate free space optical communications links. This project made use of a retroreflector modulator design which redirected a laser beam back on itself as the retroreflector modulated the optical intensity. Since the principal components were already set up in a laboratory, we decided to make use of the apparatus for a preliminary concept demonstration. The only significant modifications we made to the setup were the use of a focal plane array output signal to drive the retroreflector modulator and a photodetector module with increased gain to boost the voltage signal at the end of the optical link.

A diagram of the preliminary concept demonstration based on the retroreflector modulator is shown in Figure 2. The focal plane array used for this demonstration was the Detector Array Readout Test (DART) chip, designed and built at Sandia under another project. This focal plane array is well suited to this demonstration for a number of reasons. It can be operated with very simple control electronics, requiring only one clock signal and one 5 volt DC power supply to produce the focal plane output signal. Its signal output range is approximately 1.3 - 3.5 volts, which allows direct connection to the modulator without any gain or level shifting.

Figure 3 is a photograph of the preliminary concept demonstration. The laser operated in the short wavelength infrared region of the spectrum. The photodetector is a Thorlabs model PDA255 with a 1 mm diameter InGaAs photodiode and a built-in amplifier with a transimpedance gain of 10^4 volts/amp. The specified bandwidth of the photodetector is 50 MHz. We added a 1 inch diameter short focal length lens in front of the photodetector to help collect the full beam width and focus it on the 1 mm diameter photodiode. The focal plane array was operated at an output rate of 10^5 pixels/second.

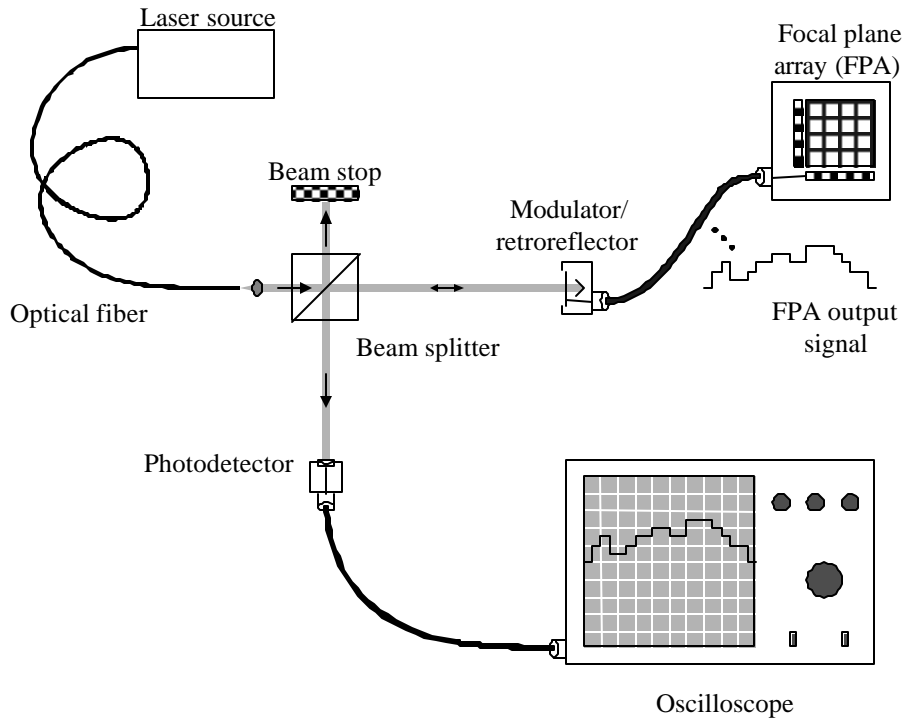


Figure 2. Modulator/retroreflector concept diagram

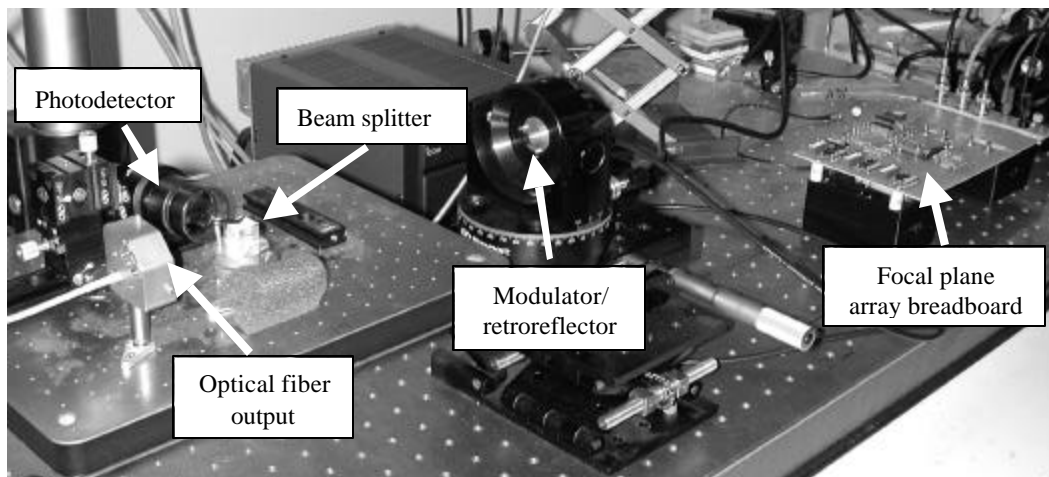


Figure 3. Preliminary concept demonstration

Results of preliminary demonstration

The result of the preliminary demonstration was somewhat successful. We were able to observe the output of the photodetector on an oscilloscope, and it was clearly a replica of the focal plane output signal. However, the peak-to-peak amplitude of the received signal was only about 56 mV, compared to the 2.2 V pk-pk amplitude of the focal plane output signal. The received signal was also quite noisy relative to its amplitude.

We investigated the weak signal by estimating the optical power received by the photodetector and comparing it with the optical power measured at several positions in the optical path. Table 1 shows the power measured with a germanium radiometer probe (3 mm diameter) at three positions in the optical path. By slightly varying the position of the radiometer probe, we were fairly certain the laser beam was underfilling the radiometer probe and the numbers shown represent the total optical power in the beam. The third row in Table 1 shows the input to the PDA255 detector with zero volts on the modulator. The loss at this point is fairly large, but is consistent with a 3 dB loss through the beam splitter and the loss due to the small size of the modulator/retroreflector. The last line shows the signal power collected by the PDA255 detector with zero volts on the modulator. The output signal voltage was referenced back to received power using the data sheet responsivity of 8,200 volts/watt at the operating wavelength. The loss at this point is probably due to reflection off the uncoated collecting lens and less than ideal focusing of the beam spot onto the small detector area. The measured losses at each point were consistent with our expectations. However, the laser power input to the beam splitter was much lower than the 20 mW or so we had anticipated.

Table 1. Optical Power Measurements

	Measured Power (mW)	Coupling Factor	Loss (dB)
Input to Beam Splitter	0.8390		
Input to Modulator	0.4400	0.5244	-2.8
Input to Detector	0.0290	0.0659	-11.8
Signal from Detector	0.0195	0.6728	-1.7

We also performed a quick measurement of the transfer curve of the optical power input to the detector as a function of modulator voltage. The results are shown in Figure 4.

The output voltage range for the DART focal plane array is approximately 1.3 - 3.5 volts. Given the detector signal at zero modulator voltage from Table 1, the detector responsivity, and the transfer function of Figure 4, the estimated peak-to-peak signal output using the DART array and the modulator/retroreflector agreed very closely with the measured amplitude of 56 mV.

After making these measurements we were fairly confident we understood the optical throughput of the preliminary demonstration setup. We showed that the focal plane output signal could be transmitted over an optical link. With greater input laser power and a more efficient modulator design, a modulated signal amplitude approaching 1 volt should be possible.

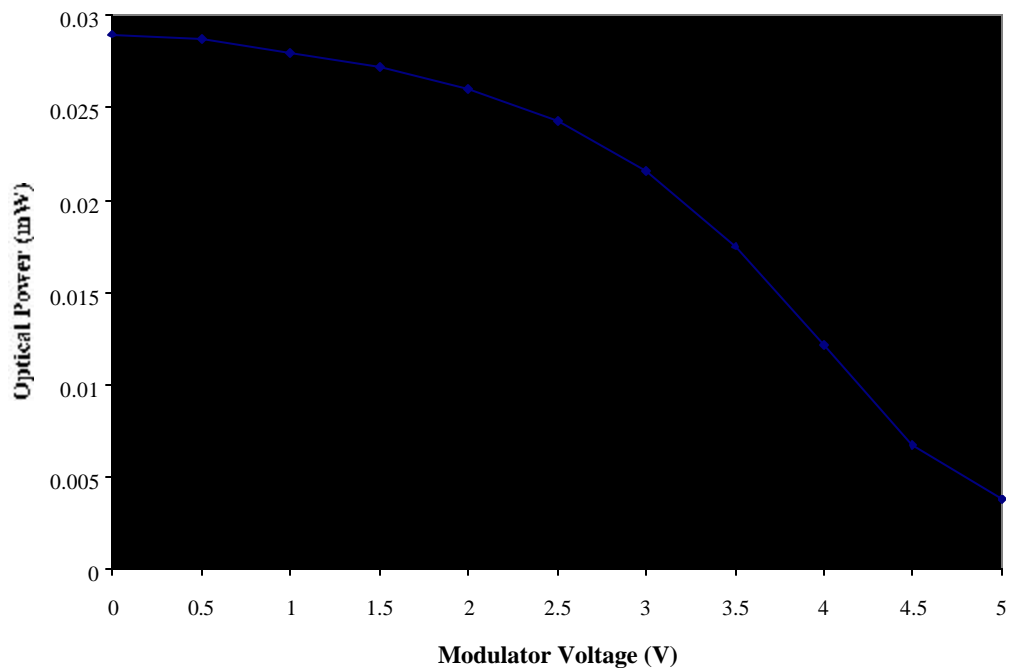


Figure 4. Modulator/retroreflector transfer function

Optical Interconnect Breadboard

Breadboard description

The chief difference between our optical interconnect breadboard and the preliminary demonstration setup was the modulator design. The modulator in our breadboard was a simple planar reflector rather than a retroreflector. In addition, the modulator for the breadboard operated at a shorter wavelength, approximately 850 nm. This modulator was also fabricated at Sandia for another program and we were able to obtain one for our use. One of the drawbacks of this particular modulator was its large size, 4 mm x 4mm. Although such a large modulator area made optical alignment very easy, its large capacitance limited the electrical bandwidth and was counter to our desire for a low power device. We proceeded with the optical interconnect breadboard with the assumption that a real system application of optical focal plane interconnection would use an optimized modulator with much lower capacitance.

To simplify the breadboard approach it was designed for room temperature operation. We realize that operating the focal plane and modulator at cryogenic temperature would require a change in the operating wavelength of the optical link or a redesign of the modulator to correct for the expected change in wavelength with temperature. In addition to this, some study of the reliability of the device over large temperature variations and of the packaging design would be required. We think these issues are relatively straightforward to resolve and do not affect the viability of the optical interconnection concept.

Other than the reflectance modulator, all the components for the optical interconnect breadboard are commercially available. A diagram of the optical interconnect breadboard is shown in Figure 5. Continuous wave optical illumination is provided by a SDL-5401 laser diode installed in a Newport model 700 temperature controlled mount with collimating optics option. A Newport model 505 laser diode driver and a model 350 temperature controller provide inputs to the laser diode and maintain the desired temperature. The output from the laser diode is couple into an optical fiber for ease of positioning near the modulator. The optical fiber has a GRIN (GRaded INdex) rod at its output end to provide relatively low beam divergence. The beam reflected off the the modulator is received by the same Thorlabs PDA255 photodetector module described earlier. The output signal from the photodetector is sent to a computer controlled data acquisition system that is typically used for focal plane array output signals. This system provides for digitization, storage, and analysis of focal plane array data.

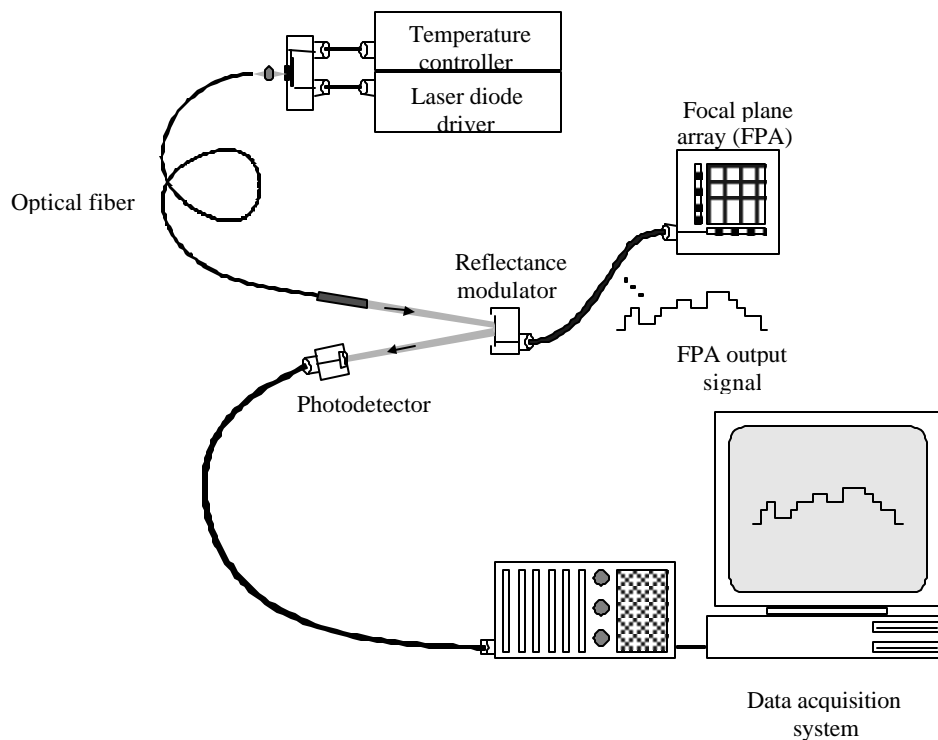


Figure 5. Optical interconnect breadboard concept

A photograph of the optical interconnect breadboard setup is shown in Figure 6 and a close-up photograph of the fiber collimator, reflectance modulator, and photodetector is shown in Figure 7.

The following sections provide more details about the breadboard components and the measurements made to characterize their performance.

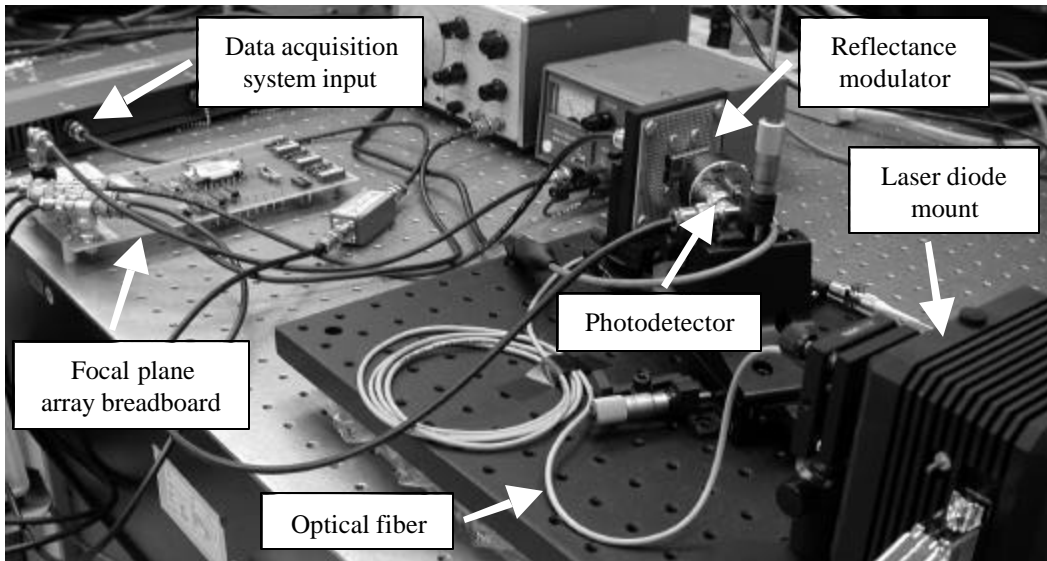


Figure 6. Optical interconnect breadboard setup

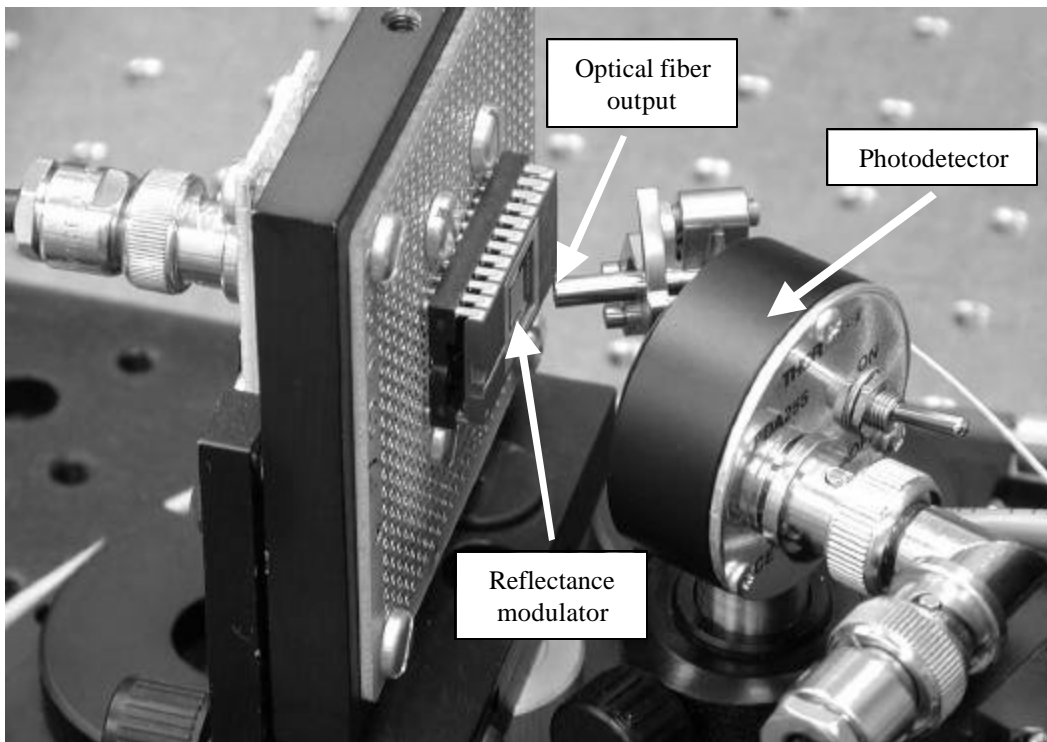


Figure 7. Close-up of reflectance modulator

Reflectance modulator

The MQW reflectance modulator is the key component of this particular approach to optical interconnection of focal plane array output. The modulator must exhibit a substantial variation

in its reflectance as the voltage on the device is changed, and the voltage required to alter the reflectance should be on the order of a few volts or less. For an actual optical interconnect application the device capacitance should be small to reduce the drive requirements on the focal plane output amplifier. As mentioned above, the reflectance modulator we were able to obtain for this breadboard demonstration was larger than needed (4 mm x 4 mm) and had a much larger capacitance than desired. The minimum area required for the modulator depends on the optical spot size on the device. A larger modulator would make alignment easier and would reduce the effects of mechanical vibration.

The MQW reflectance modulator operates over a narrow wavelength range. We measured the reflectance versus wavelength at different modulator voltages using a monochromator to determine the optimum laser wavelength. The results are shown in Figure 8.

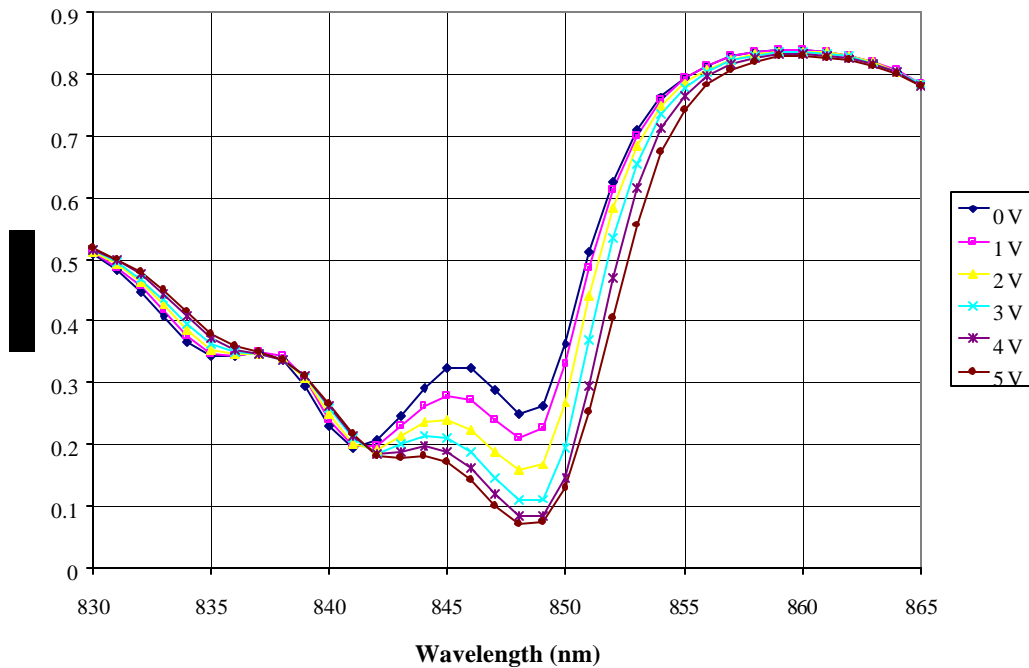


Figure 8. Modulator reflectance versus wavelength

We can define a modulation factor, M , for two voltages, V_{\min} and V_{\max} . If $r(V)$ is the reflectance for a given modulator voltage, the modulation factor is

$$M = \frac{r(V_{\min}) - r(V_{\max})}{r(V_{\min})}$$

A high modulation factor is desirable because it reduces the DC offset in the received signal and simplifies the requirements for downstream gain and offset adjustments. The modulation factor

is plotted in Figure 9 for a 1 to 3 volt and a 2 to 4 volt signal range. From these plots, the optimum wavelength appears to be 849 nm.

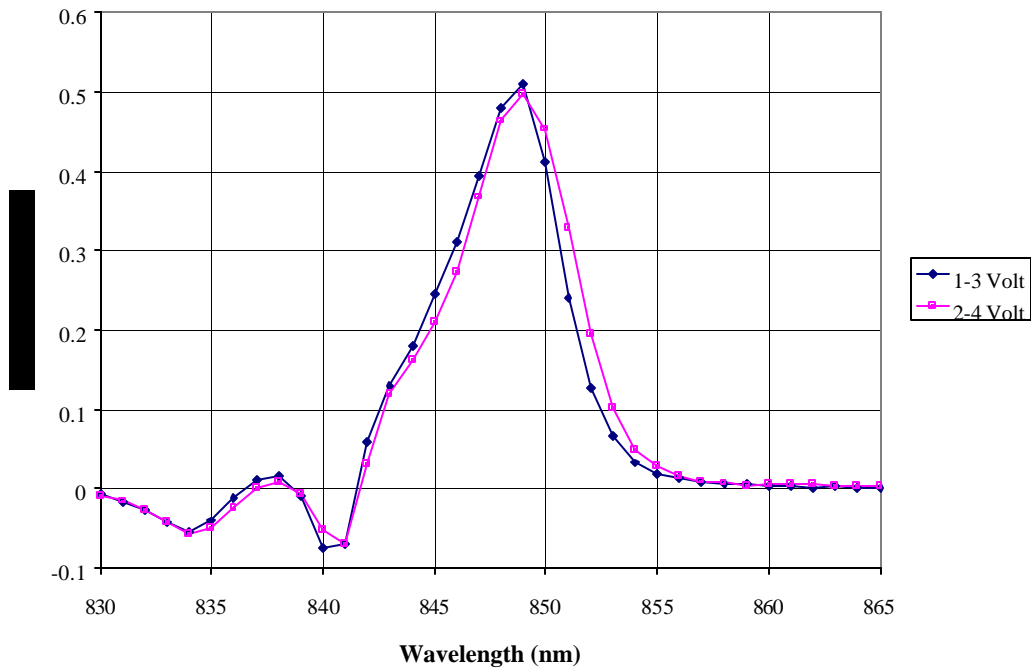


Figure 9. Modulation factor versus wavelength

Modulator reflectance versus voltage was measured at 849 nm and is shown in Figure 10.

We measured the reflectance modulator's capacitance as a function of modulator voltage. Since the modulator is a reverse biased PIN diode, we expected the capacitance to decrease with increasing operating voltage. The results of the capacitance vs. voltage measurements at 100 kHz and 1 MHz are shown in Figure 11. For the output voltage range of a typical focal plane array, the modulator capacitance is roughly 3,000 pF. Assuming a modulator of 500 μm diameter, a size more appropriate for focal plane optical interconnection, the capacitance would scale to 37 pF. Further refinements in modulator design could perhaps decrease the capacitance per unit area.

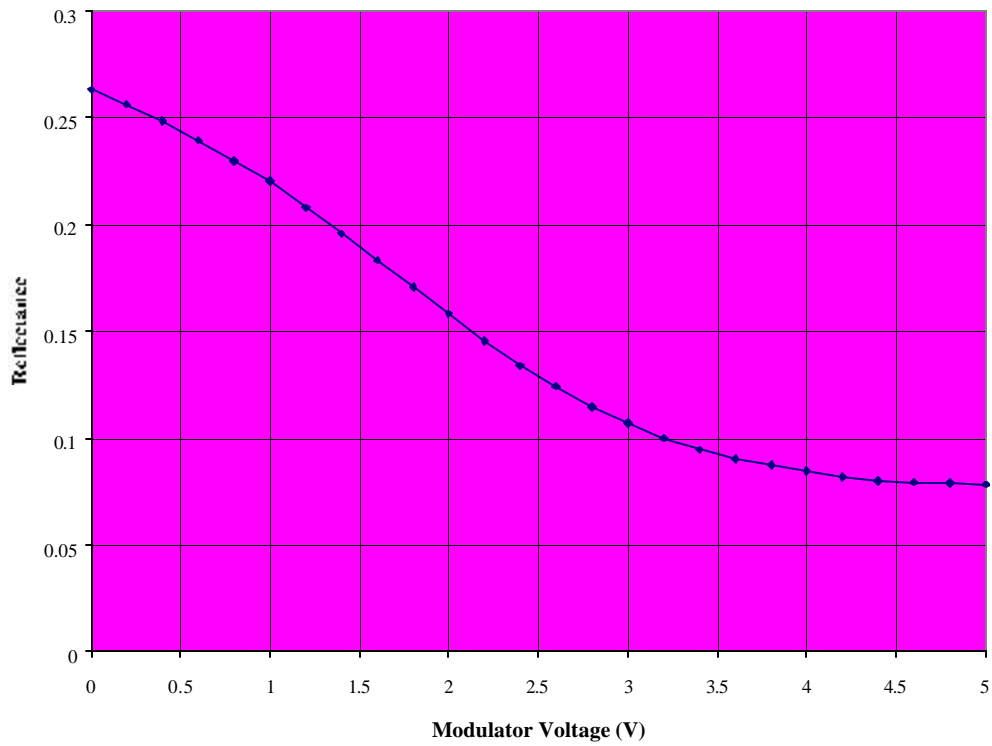


Figure 10. Modulator reflectance versus voltage at 849 nm

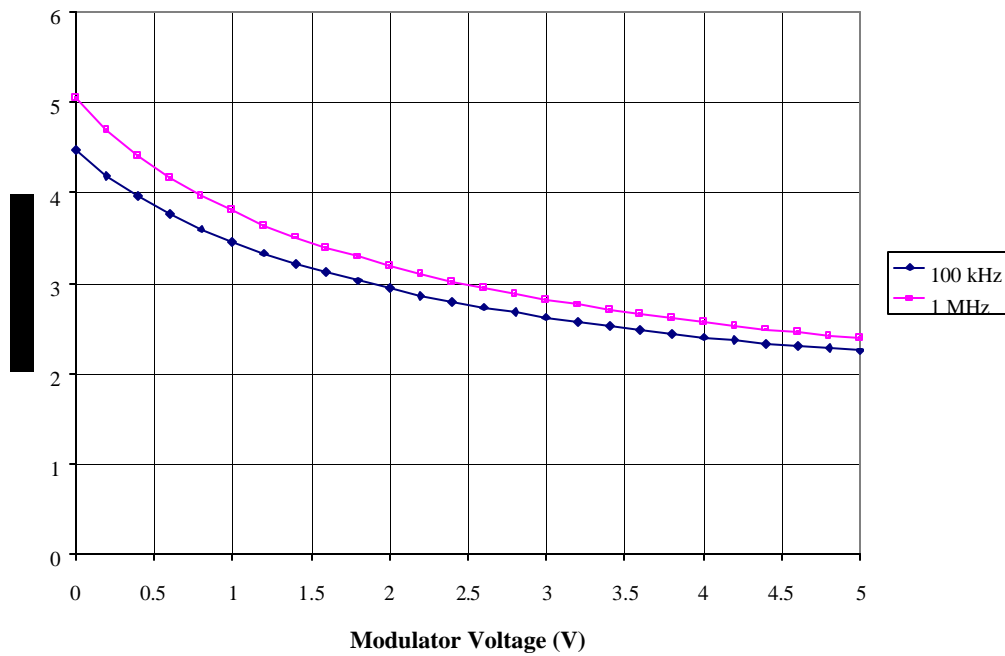


Figure 11. Reflectance modulator capacitance versus wavelength

While experimenting with the breadboard apparatus, we became aware that laser illumination on the reflectance modulator produced a photocurrent. This is not surprising since the device is a PIN diode. We measured the spectral responsivity and quantum efficiency of the modulator at 2 volts bias, and the results of the quantum efficiency measurements are shown in Figure 12. It is notable that the quantum efficiency is above 30 percent at the operating wavelength, and substantial photocurrent is generated as the incident laser power is increased to produce a larger signal.

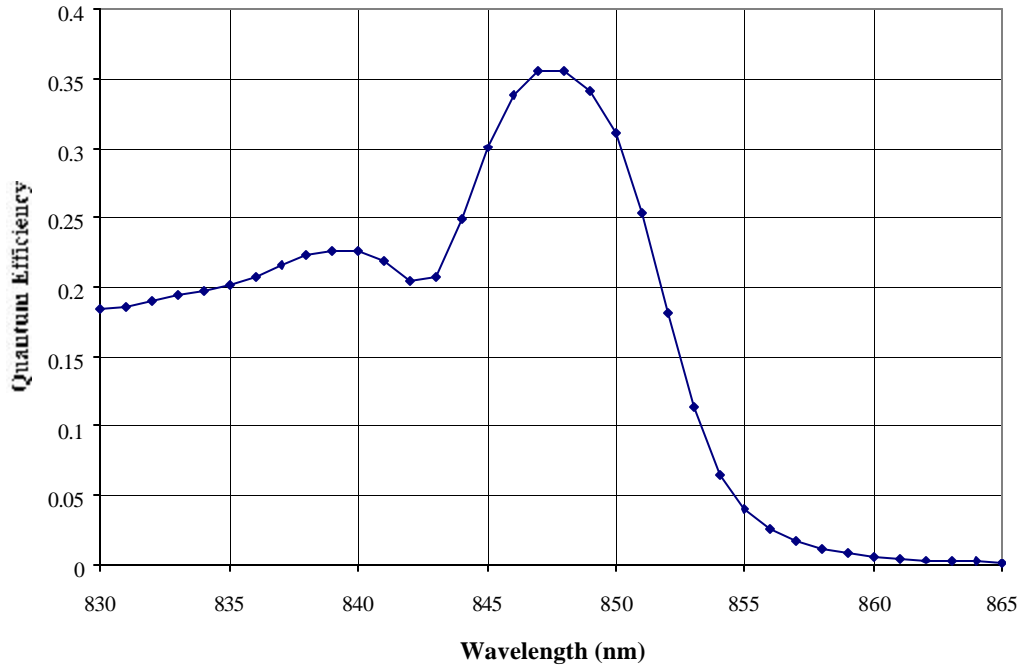


Figure 12. Modulator spectral quantum efficiency at 2 volts reverse bias

Laser diode source

Second only to the modulator performance characteristics, the noise of the laser source is a critical aspect of the selected optical interconnect concept. Lasers for optical communication can be characterized by a relative intensity noise (RIN) parameter. Since the fields of optical and radio frequency data links deal mostly with noise and signal power ratios, the RIN parameter is a noise power to signal power ratio normalized by the noise bandwidth, Δf . If p_{laser} is the root mean square laser intensity variation, and P_{laser} is the laser power, RIN is defined as

$$\text{RIN} = \frac{p_{\text{laser}}^2}{P_{\text{laser}}^2} \cdot \frac{1}{\Delta f}$$

This normalized power ratio is usually expressed in dB/Hz.

Semiconductor diode lasers are known to be susceptible to intensity fluctuations, mode hopping, and other instabilities, especially when back reflections introduce unwanted feedback into the lasing cavity. Solid state lasers, such as Ti:Sapphire, can have lower RIN values than diode lasers, but their efficiency is lower as well. A good solid state laser may have a RIN value better than -160 dB/Hz. Since the objective of this project was to demonstrate a low power optical link for satellite applications, we chose to use a temperature controlled diode laser and find out how well it could perform.

Given our experience with the preliminary demonstration apparatus and the lack of available optical power, we chose a laser diode with plenty of power. The SDL-5401 we selected has a maximum power output of 50 mW, which was more than enough to overcome any optical losses we anticipated for the breadboard setup. The specified output wavelength is $852 \text{ nm} \pm 4 \text{ nm}$ with a temperature coefficient of wavelength of $0.3 \text{ nm}/^\circ\text{C}$. After receiving the laser diode we measured the output wavelength as a function of temperature using an Alton Instruments LM-30 wavelength meter. The results are shown in Figure 13. The measurement was limited by the resolution of the wavelength meter, but it was clear that the desired operating temperature for 849 nm output is around 26-27 °C. The measured temperature coefficient of wavelength is close to $0.2 \text{ nm}/^\circ\text{C}$, somewhat lower than specified.

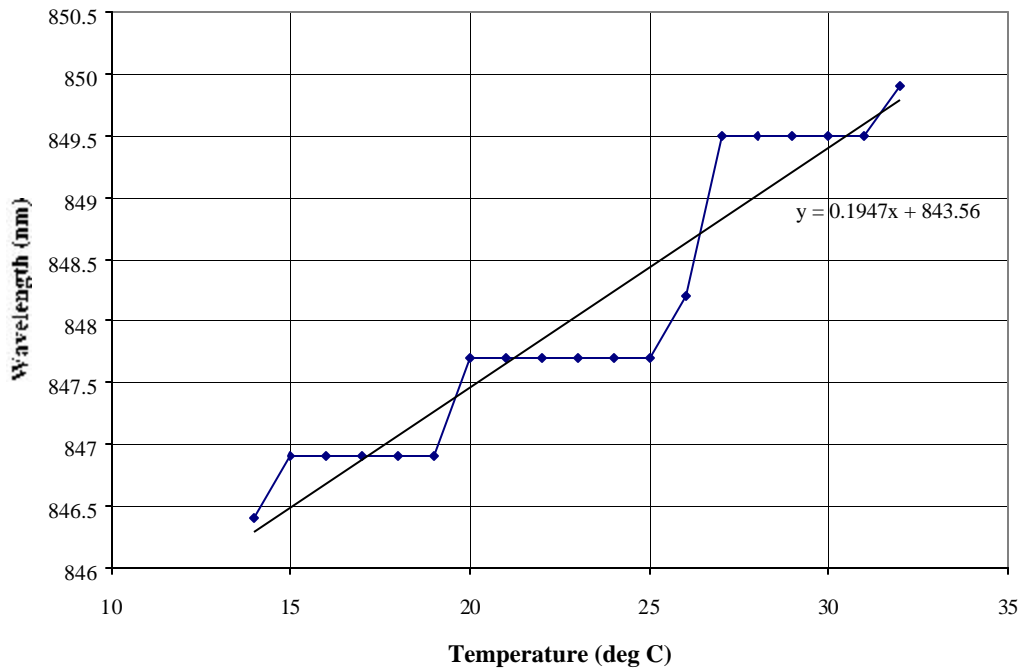


Figure 13. Laser diode output wavelength versus temperature

We observed some of the undesirable characteristics of diode lasers with the breadboard setup. We found that active temperature control of the laser diode helped to reduce mode hopping and overall laser intensity noise. Choice of the precise operating temperature was achieved through a balance of output wavelength and observed laser stability. Laser noise was found to vary

considerably over periods of several minutes, but we were able to make measurements lasting a few seconds during the relatively quiet intervals.

We made several measurements of laser noise at various places in the breadboard optical path using the PDA255 photodetector. The results of our laser noise measurements are shown in Table 2. We define a laser relative noise (LRN) parameter, which is simply the ratio of the RMS voltage noise of the photodetector with the laser on, s_{laser} , relative to the laser signal, S_{laser} . LRN is related to RIN by the following equation.

$$\text{LRN} = \sqrt{\text{RIN} \cdot \Delta f}$$

Table 2. Laser Noise Measurements

Measured at output of:	S_{laser} (mV)	s_{laser} (mV)	LRN	RIN (dB/Hz)
Laser diode	1473	0.923	6.266E-04	-136.6
Fiber collimator	2292	1.748	7.626E-04	-134.9
Modulator (open circuit)	1516	1.523	1.005E-03	-132.5

The increase in laser relative noise at points further along the optical path may indicate the effects of optical feedback and mechanical vibration. There are some well known techniques to improve RIN, such as antireflection coatings, optical isolators, and angle polished fiber connectors. We could also have the laser diode coupled to an angle polished fiber pigtail.

Fiber optics

The temperature controlled laser diode mount included an optical collimator with medium precision x, y, and z adjustment capability. The collimated beam was transmitted over a short distance (less than 1 cm) to a collimating optic assembly (Thorlabs F220FC-B) installed in a tip-tilt mount. Multimode optical fiber with 65.5 μm core diameter was used to deliver the beam to the reflectance modulator. Rather than varying the laser diode current to change the delivered optical power, we purposely defocused and misaligned the fiber optic input.

The output end of the optical fiber included a GRIN rod output collimator to reduce beam divergence. The output collimator was positioned about 1 cm from the optical modulator and tilted with respect to it to provide an angle of incidence roughly 10 degrees from normal.

Photodetector

The Thorlabs PDA255 high speed photodetector was briefly described in the description of the preliminary concept demonstration. The 1 mm diameter InGaAs photodiode coupled with a transimpedance amplifier using a 10 k Ω feedback resistor has a data sheet responsivity at 850 nm of about 2,000 volts/watt. We did not use a collecting optic in front of the detector because the beam divergence was low and the beam path was short. Higher responsivity could have been achieved if we had procured a similar photodetector using a silicon photodiode.

The electronic bandwidth of the photodetector module is 50 MHz, but we used a simple RC low pass filter at the input to the data acquisition system. We typically use such a filter when testing

focal plane arrays to limit the noise bandwidth while allowing enough signal bandwidth to permit adequate settling between pixel values. For these tests the noise bandwidth was limited to 17.9 MHz.

The maximum RMS noise given in the data sheet of the PDA255 photodetector is 2.0 mV. We think it's possible to do better than this with a custom designed photodiode and amplifier. With the reduced noise bandwidth provided by the low pass filter, the calculated maximum noise is approximately 0.95 mV.

Measured Breadboard Performance

With all the components of the breadboard system set up and aligned, we proceeded with the demonstration of optical interconnect performance. We allowed the laser diode to stabilize while operating at 25.9 °C. Operation of the DART focal plane array was started and its output was connected to the reflectance modulator. We observed the output from the optical interconnect link on an oscilloscope and compared it with the input direct from the focal plane array. An oscilloscope photo with both output and input is shown in Figure 14. The upper trace shows the optical interconnect output on a 500 mV per division scale. The lower trace is the inverted input from the focal plane at 1 V per division.

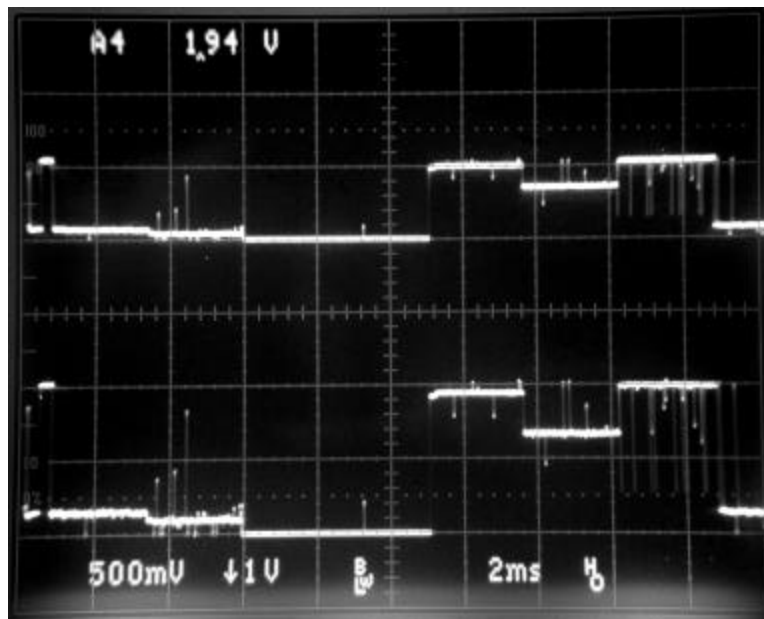


Figure 14. Optical interconnect output and DART focal plane output

The traces show approximately 1 frame of data for the 128 row x 16 column test array. The DART test array is composed of 8 subarrays of 16 x 16 pixels each, which represent various unit cell design approaches. This creates regions of the output waveform at substantially different voltage levels. The isolated spikes in the output waveform are due to individual bad pixels which deviate from the normal output level for a given subarray. These bad pixels are actually quite useful for assessing the adequacy of the electronic bandwidth of the output amplifier and data acquisition system.

The voltage modulation at the output of the optical link is smaller than the input voltage modulation. It was assumed we could simply increase the laser power to achieve a larger output voltage swing. We found, however, that there was a limit to the optical power illuminating the modulator while maintaining link operation. When the optical power was increased to produce an output voltage swing greater than about 0.6 volts, the input signal from the DART array and the optical interconnect output signal became very unstable and both collapsed at higher input signal levels.

We think this optical power limit is due to photocurrent generated in the reflectance modulator. Recalling that the absorption quantum efficiency of the modulator is over 30 percent in this wavelength region, approximately 200 μA of photocurrent is produced for each milliwatt of laser power incident on the modulator. Given the polarity of the modulator PIN junction, this photocurrent must be supplied by the output amplifier of the focal plane array in order to maintain the input signal voltage. If this photocurrent cannot be supplied by the focal plane output amplifier, the voltage on the input sags to a lower level. For photocurrent above a certain level the focal plane array output amplifier is not able to generate any significant input signal to the optical link.

Photocurrent generated in the reflectance modulator also limits the maximum pixel rate. The traces in Figure 14 were obtained at a pixel rate of 100 kilopixels per second. Although we typically operate the DART array at an output rate of 1 megapixel per second, both the input from the DART array and the optical interconnect output were distorted at the higher pixel rate, as shown in Figure 15.

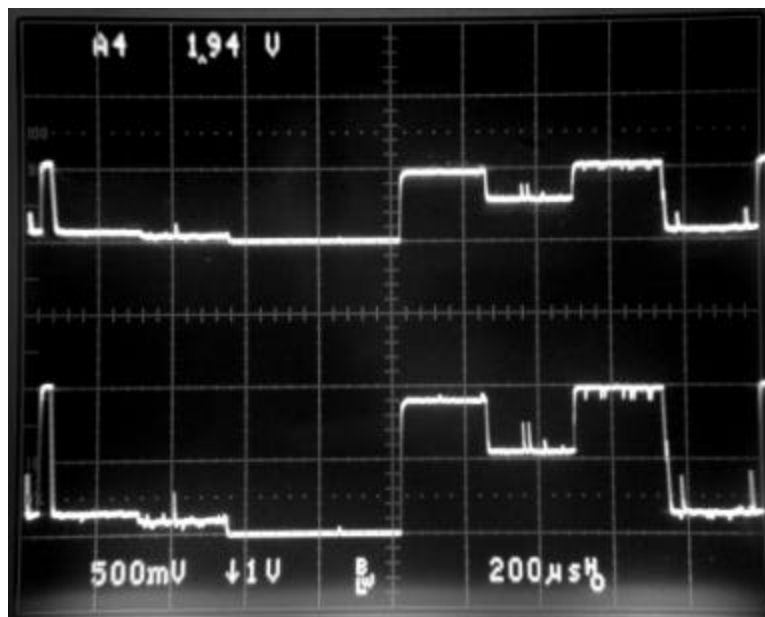


Figure 15. Output traces at 1 megapixel/second

To gain insight into what may be happening, Figure 16 shows 1 megapixel per second input and output traces at an expanded time base. The waveforms of the bad pixels are clearly skewed and seem to be limited by the slew rate in one direction rather than an RC time constant. The lower trace representing the input from the DART focal plane has been inverted relative to the actual focal plane output, so the slew rate limit appears as the focal plane signal attempts to change from a lower to a higher voltage. This is what one would expect if the output amplifier is trying to supply the modulator photocurrent as well as driving to a higher voltage. For the higher to lower signal transition, the photocurrent actually aids the transition speed and the slew rate is very fast.

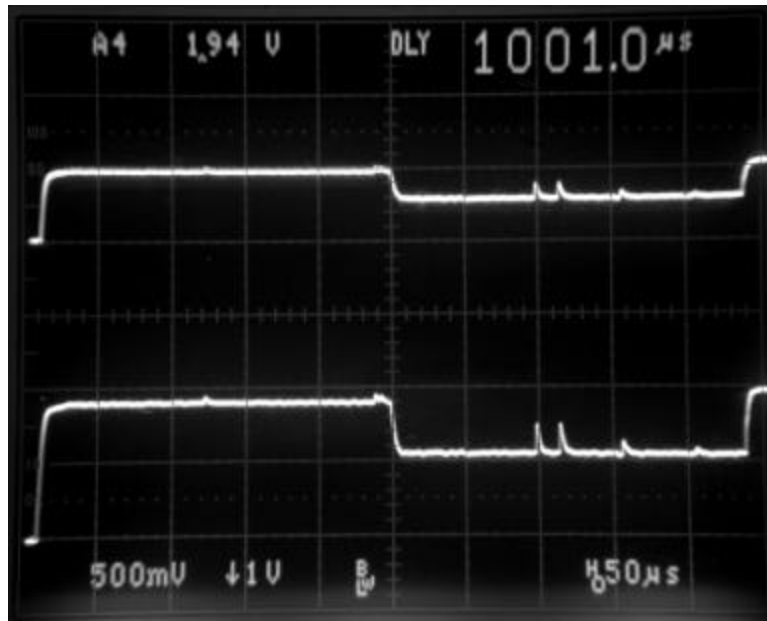


Figure 16. Expanded 1 megapixel/second output trace

To characterize the overall performance of the optical interconnect breadboard, we made a series of signal and noise measurements at different laser power levels. We made use of our focal plane array data acquisition system to digitize and store the data and to calculate RMS noise and signal amplitude. The RMS noise was determined by calculating the temporal standard deviation for each pixel over 128 frames and then finding the median value for all the pixels in the subarray. Because of the variety of subarrays on the DART focal plane array and different polarities of unit cell designs, certain subarrays are at the minimum voltage level and other subarrays are at the maximum level. Therefore, each frame of input signal from the array spans the available input voltage range. The total signal swing at both the input and output can be determined from the oscilloscope waveforms without changing the light level incident on the focal plane. All the following measurements were made with the focal plane in the dark.

We measured the DART focal plane output voltage swing, ΔV , and noise voltage, v , under various conditions and calculated the signal to noise ratio. The results are shown in Table 3. Loading of the focal plane output amplifier by the laser induced modulator photocurrent is evident. Laser power on the modulator also increases the focal plane output noise level,

probably through coupling of laser intensity noise to the output voltage level through variations in the photocurrent. With the laser off, the modulator provides a bit of noise filtering because of its large capacitance. This may explain the slightly higher noise when the modulator is disconnected.

Table 3. DART FPA Signal and Noise Levels

	ΔV (mV)	v (mV)	$\Delta V/v$
Modulator connected, laser on	2100	1.23	1710
Modulator connected, laser off	2266	0.97	2333
Modulator disconnected	2266	0.99	2286

We then measured the signal swing, ΔS , and noise voltage, s_{noise} , for the optical interconnect output at 4 different laser power levels and calculated the signal to noise ratio. To quantify the noise added by the optical interconnect link, we compare the voltage SNR at the focal plane output when the modulator was disconnected to the voltage SNR at the optical interconnect output. SNR is degraded through the optical link by a factor of 10 or more. This ratio expressed in dB is the link noise figure, LNF. These results are shown in Table 4.

Table 4. Optical Interconnect Signal and Noise Levels

	ΔS (mV)	s_{noise} (mV)	$\Delta S/s_{\text{noise}}$	$\text{SNR}_{\text{in}}/\text{SNR}_{\text{out}}$	LNF
Trial 1	170.9	1.24	137.6	16.61	24.4
Trial 2	258.8	1.45	179.1	12.77	22.1
Trial 3	449.2	1.91	235.1	9.73	19.8
Trial 4	600.6	2.57	233.9	9.78	19.8

Analysis of Measurements

Calculated signal swing

We can analyze the throughput of the optical interconnect breadboard, and determine if the measured output signal levels are reasonable. Let α represent the coupling efficiency of the light reflected by the modulator and received by the photodetector. Letting R represent the voltage responsivity (volts/watt) of the photodetector and recalling that $r(V)$ is the modulator reflectance as a function of voltage, the output signal swing when the input changes from V_{min} to V_{max} is

$$\Delta S = \alpha \cdot P_{\text{laser}} \cdot R \cdot [r(V_{\text{min}}) - r(V_{\text{max}})]$$

After the four measurement trials the optical power was adjusted to provide an output signal swing of roughly 500 mV. The laser power at the output collimator just ahead of the reflectance modulator was measured to be 2.39 mW. With the DART focal plane array connected to the modulator and the laser running, V_{min} and V_{max} were measured to be 1.18 V and 3.28 V,

respectively. Using reflectance values interpolated from Figure 10 and a voltage responsivity of 2,000 volts/watt, the coupling efficiency was calculated to be greater than 90%.

The laser power incident on the modulator for most of these measurements was much lower than the maximum power available from the laser diode. We attenuated the optical power at the modulator by purposely misaligning the optical input coupling to the fiber. To evaluate the minimum optical loss, we tweaked the input coupling and measured the power into and out of the optical fiber. At a laser diode temperature of 25.9 °C and a drive current of 50 mA, the measured optical power out of the laser diode collimating optic was 38.6 mW. The measured power out of the fiber just ahead of the modulator was 22.55 mW, for a coupling efficiency of 0.584 (-2.3 dB). A much lower power laser diode would be used in an actual optical interconnect application.

Calculated noise

The components of the total output noise we consider are FPA noise at the input to the optical interconnect, photodetector dark noise due to its amplifier, photodetector shot noise, and laser intensity noise. To compare the calculations with measured data, we express the noise as a function of output signal swing, ΔS . All these noise sources depend on ΔS except for photodetector amplifier noise. For this analysis, data acquisition system noise is included with photodetector noise. The noise of the photodetector under dark conditions, s_{det} , was measured to be 1.11 mV.

Photodetector shot noise, s_{shot} , increases as the square root of the photocurrent generated in the sensing element, and is given by the equation

$$s_{shot} = R_{fb} \sqrt{2 \cdot q \cdot I_{photo} \cdot \Delta f} = \sqrt{2 \cdot q \cdot \alpha \cdot P_{laser} \cdot R \cdot R_{fb} \cdot r(V) \cdot \Delta f}$$

R_{fb} is the feedback resistor value of the photodetector transimpedance amplifier. Using the relationship between laser power and output signal swing, and defining $\beta(V) = r(V) / [r(V_{min}) - r(V_{max})]$, we have

$$s_{shot} = \sqrt{2 \cdot q \cdot R_{fb} \cdot \beta(V) \cdot \Delta f \cdot \Delta S}$$

For the reflectance modulator used and the DART array output voltage range, $\beta(V)$ varies between 0.879 at V_{max} to 1.879 at V_{min} . The noise measurements corresponded to a portion of the output signal which was at V_{max} , so the minimum value of β was used in the noise calculation.

Noise voltage present at the FPA output is amplified or attenuated by the link gain, which is defined as the ratio of ΔS to ΔV . FPA noise, s_{fpa} is simply

$$s_{fpa} = \frac{v}{\Delta V} \cdot \Delta S$$

The output noise due to laser intensity noise is given by

$$s_{\text{laser}} = \alpha \cdot \text{LRN} \cdot P_{\text{laser}} \cdot r(V) \cdot R$$

Expressing this in terms of ΔS , we have

$$s_{\text{laser}} = \beta(V) \cdot \text{LRN} \cdot \Delta S$$

Laser relative noise measured at the output of the modulator was used for the noise calculation. As given in Table 2, the LRN at this location in the optical interconnect is 1.005E-03.

Total noise variance for the optical interconnect output is, therefore

$$s_{\text{total}}^2 = s_{\text{det}}^2 + (2 \cdot q \cdot R_{\text{fb}} \cdot \beta(V) \cdot \Delta f) \cdot \Delta S + \left[\left(\frac{v}{\Delta V} \right)^2 + (\beta(V) \cdot \text{LRN})^2 \right] \cdot \Delta S^2$$

(Total noise equation)

We can compare the total output noise predicted by this expression with the measured noise at the four different ΔS values achieved by varying the laser power. Predicted noise and measured noise are shown in Figure 17.

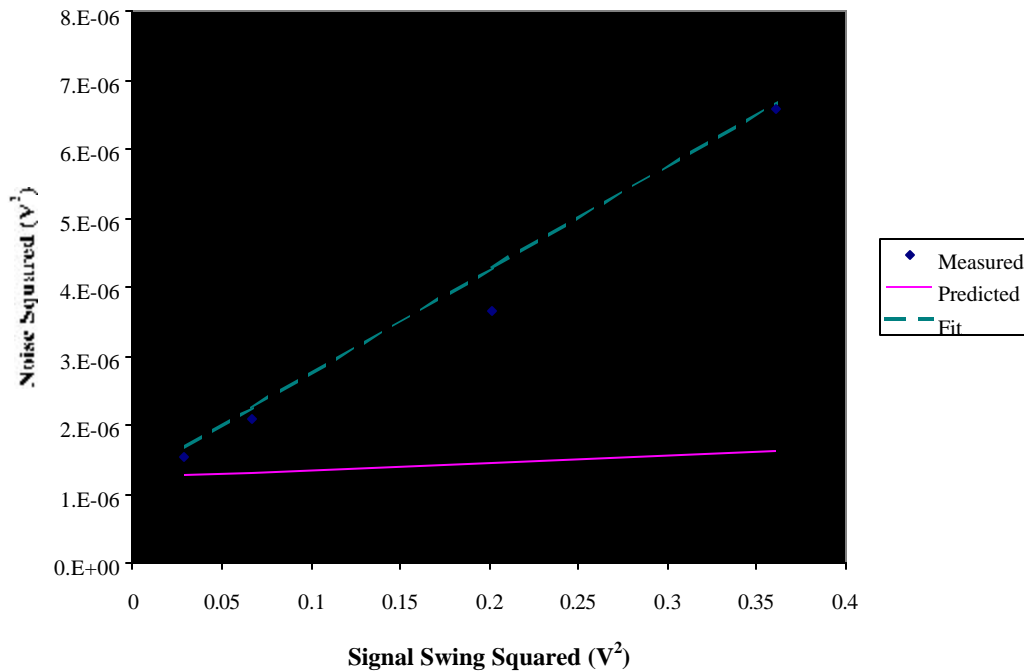


Figure 17. Noise squared versus signal swing squared

The measured data points show a linear relationship between noise and signal as predicted by the total noise equation, but the predicted slope is much less than that determined by the measured data. Using the slope of the trend line applied to the measured data, the value of LRN implied by the output noise data is $4.377\text{E-}03$, a factor of 4.36 greater than the measured LRN. The line labeled “Fit” in Figure 17 represents the noise recalculated to fit the effective LRN determined by the output noise data.

The cause for this discrepancy has not been determined, but we observed that laser noise varied considerably during our measurements. There is also the possibility of photocurrent generated in the modulator affecting the noise output of the FPA and leading to an increase in the effective LRN.

Using an effective LRN term which tracks the measured data, we can examine the noise sources to determine the dominant ones. Figure 18 shows the components of the total squared noise for the four values of ΔS . Detector noise and laser noise are the dominant contributors to output noise.

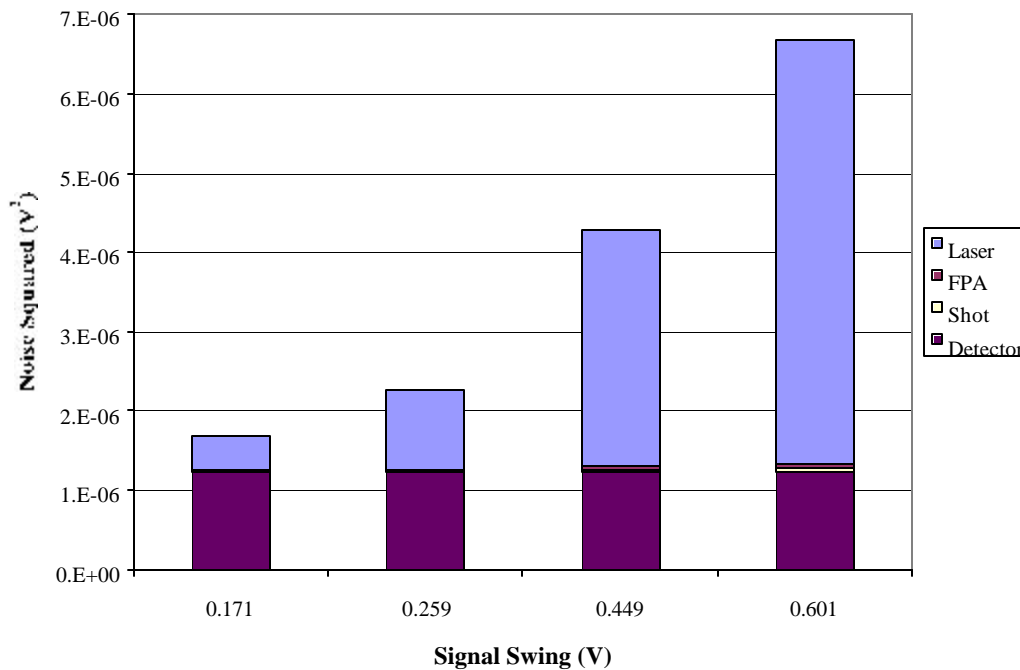


Figure 18. Components of squared noise

From the total noise equation, we see that the ratio of noise to signal swing, $s_{\text{total}}/\Delta S$ approaches a constant value at large values of ΔS and is dominated by LRN.

Potential performance improvement

Examination of the equation for total noise allows us to determine the potential performance improvements that can be made. One of the goals for design of an optical interconnect system is to minimize the degradation in SNR from link input to link output. The first priority is reduction in laser relative noise. Inspection of the total noise equation indicates that LRN should satisfy the following inequality

$$\text{LRN} \ll \frac{v}{\Delta V \cdot \beta(V)}$$

For the DART array signal and noise values and the β value of the reflectance modulator, LRN should be much less than 4.975E-04. This corresponds to a value for RIN of -138.6 dB/Hz. The LRN measured directly from our laser diode approached this level, but the apparent increase in LRN evident in the output noise was substantially higher.

Assuming LRN is reduced sufficiently, the shot noise term determines the value of ΔS needed to keep it from limiting SNR. The following inequality determines the minimum signal swing required.

$$\Delta S \gg (2 \cdot q \cdot R_{fb} \cdot \beta(V) \cdot \Delta f) \cdot \left(\frac{\Delta V}{v} \right)^2$$

For the values applicable to our breadboard system, ΔS should be much greater than 264 mV.

To achieve optimum performance, the detector noise also needs to be reduced. For a situation where the shot noise and laser noise contributions are small, the detector noise should meet the following requirement

$$s_{\text{det}} \ll v \cdot \frac{\Delta S}{\Delta V}$$

As with the shot noise term, the detector noise term calls for a larger value of ΔS to optimize performance. Any parameter that increases link gain will reduce the effect of detector noise. The photodetector used for the breadboard setup was not optimized for the wavelength used. A factor of 3 improvement in ΔS could be easily achieved using a silicon photodetector. Higher transimpedance gain may also help the situation. However, the required electronic bandwidth may be difficult to achieve with a single amplifier stage. Multiple amplifier stages could be used to boost ΔS while maintaining bandwidth.

Figure 19 illustrates the performance improvement that could be achieved if laser intensity noise and detector noise are reduced below the other noise sources. The first curve shows SNR versus signal swing for the total noise calculated with the LRN figure derived from the output noise data. This curve corresponds to the noise levels measured in our breadboard setup. The second curve shows the limit to SNR imposed by the high level of laser intensity noise. The third curve shows the SNR level that could be achieved if laser noise and detector noise are reduced to levels

where only shot noise and FPA noise remain. The fourth curve shows the limit to SNR governed by the FPA noise level at the input to the optical link.

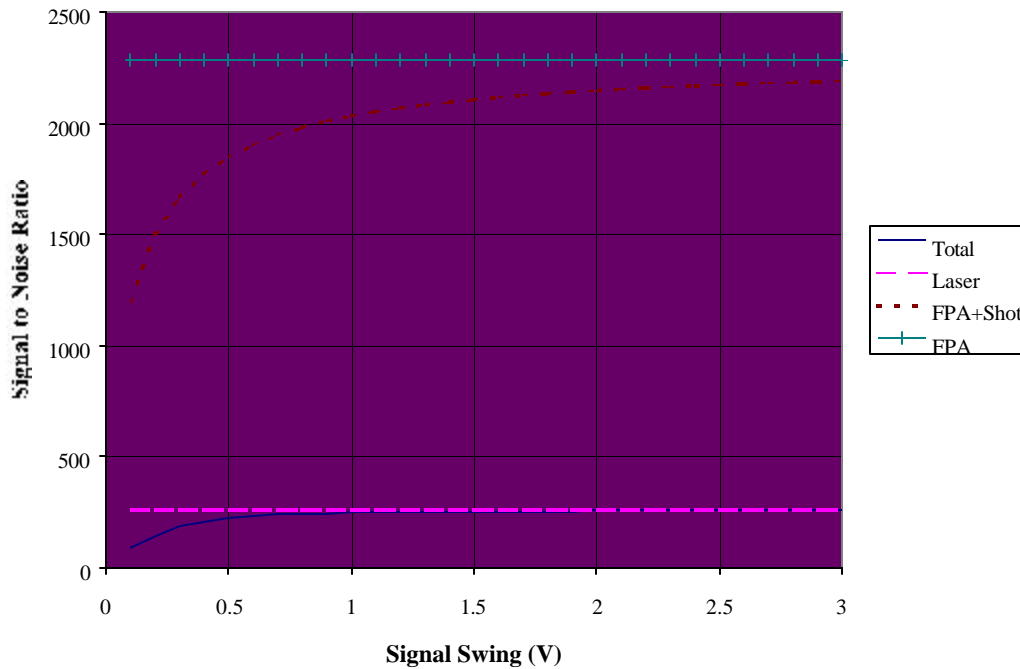


Figure 19. Component SNR versus output signal swing

Suggestions for Further Work

Improved source

From the above analysis it is clear that a low noise laser source is required. A RIN value approaching -160 dB/Hz is a goal. As stated earlier, the compactness and high efficiency of semiconductor diode lasers are attractive, but a substantial improvement in their intensity noise needs to be achieved. Solid state lasers should also be investigated to determine if their efficiency can be made high enough to be used for an optical link without increasing total system power. With careful selection of the laser source for lower intensity noise, the link noise figure could be lowered substantially.

Improved modulator

The primary motivation for this work is to decrease the power required by the FPA output amplifiers. The capacitance per unit area for the modulator used in this project is fairly high. It would be desirable for modulator capacitance to be on the order of a few picofarads for a 500 μm diameter device.

The photocurrent produced by the MQW modulator is troublesome and imposes a current load on the FPA output amplifier. Even if higher overall reflectance could be achieved, the desire for

a large modulation factor would lead to higher absorption and greater photocurrent for part of the output signal range. It would be useful to investigate whether or not lower reflectance necessarily comes at the expense of higher photocurrent. If the photocurrent can be reduced, it should be possible to use greater laser power and obtain a larger output signal swing.

Lower noise detector

A careful analysis of design requirements and a custom approach to the photodetector could substantially improve performance. A photodiode with spectral response matched to the operating wavelength coupled with a low noise amplifier should easily improve on the performance of the off-the-shelf item that was used.

Design tradeoffs

Some of the other candidate concepts for focal plane optical interconnections could be investigated in future efforts. Given the issue of photocurrent generation in the reflectance modulator, on-focal-plane optical sources begin to look more attractive. If a substantial portion of the incident optical beam is converted to photocurrent that needs to be supplied by the FPA output amplifier, the low power advantage of a reflectance modulator approach is not as great. Integration and alignment challenges may be reduced using direct modulation of optical sources on the focal plane.

The system could potentially benefit from an investigation of free space versus fiber optic connections for use with cryogenic focal plane arrays. The reliability and thermal conductance issues with fibers spanning the warm to cold interface need to be studied. Free space optical coupling presents challenges in the areas of alignment and vibration control, especially when the drive for low capacitance leads to small device area.

The use of a digital optical link is also a possibility for future study. However, this approach depends on the implementation of A-to-D conversion on the focal plane. While on focal plane A-to-D conversion is becoming available for FPAs operating at room temperature, the power dissipation penalty works against this approach for cryogenic focal plane arrays.

Future efforts could look more systematically at the full trade space and identify those approaches holding the most promise. Performance requirements for individual components could be specified, and demonstrations of key device characteristics could be planned.

Summary and Conclusions

The objective of this project was to identify several concepts for focal plane optical interconnection and to demonstrate one of those concepts using an actual focal plane array output. With both a preliminary demonstration setup and an optical interconnect breadboard we successfully demonstrated transmission of focal plane array output waveforms over optical links. The remainder of the project focused on characterizing the performance of the optical interconnect breadboard and analyzing the results to understand the key performance drivers.

The optical interconnect approach we selected and demonstrated made use of a reflectance modulator fabricated with multiple quantum well technology. A CW laser source was aimed at the modulator, and the analog focal plane output signal was impressed on the reflected beam due

to the modulator's voltage dependent reflectance. The laser source was a temperature controlled diode laser operating at 849 nm. The received signal was fed into the same data acquisition and analysis system we use for focal plane array characterization.

We performed a number of measurements to assess the characteristics of the optical link output signal relative to the input signal from the focal plane array. The signal to noise ratio was degraded a factor of 10 or more by the optical link, and the maximum output signal level was limited due to photocurrent generation in the reflectance modulator and the limited current drive capability of the focal plane output amplifier.

We analyzed the noise components of the optical interconnect breadboard and identified laser intensity noise and photodetector noise as the limiting sources. The noise in the measured output signal that behaved as laser intensity noise was higher than the direct laser noise measurements would indicate. This discrepancy should be investigated further. Our analysis of noise sources established performance goals for laser sources and photodetectors for future efforts.

This project highlighted the design challenges involved with optical data links. By observing the performance of actual devices and analyzing their behavior, we are better able to refine this optical interconnection approach and to investigate alternative approaches.

DISTRIBUTION:

1	MS 0603	D. K. Serkland, 1742
1	0603	C. T. Sullivan, 1743
1	0874	M. Armendariz, 1751
1	0874	G. R. Schuster, 1751
1	0860	C. L. Smithpeter, 2618
1	0965	K. R. Lanes, 5711
1	0972	A. J. Medina, 5720
1	0972	S. M. Gentry, 5722
4	0972	M. K. Hinckley, 5722
1	0972	R. R. Kay, 5722
6	0972	J. L. Rienstra, 5722
1	0188	LDRD Program Office, 1030
1	9018	Central Technical Files, 8945-1
2	0899	Technical Library, 9616
1	0612	Review & Approval Desk, 9612 For DOE/OSTI